

# On Active Control of Flow Induced Vibrations

Jeff Borggaard  
Terry Herdman

Interdisciplinary Center for Applied Mathematics  
Virginia Tech, Blacksburg, Virginia 24061

Janos Turi

Programs in Mathematical Sciences  
University of Texas at Dallas, Richardson, Texas 75083

## Abstract

In this paper, we consider the design of active control strategies for flutter suppression in an aeroelastic system consisting of a two dimensional airfoil section with dynamics coupled to the surrounding flow. To facilitate this, a three-degree of freedom model for the airfoil section and a potential flow model for the flow are used. We present an example to demonstrate the feasibility of state feedback control.

## 1. Introduction

Coupling between the motions of a structure and the surrounding flow may lead to unwanted oscillations (e.g., flutter). Below, we present a computational framework to study flow induced motions of an aeroelastic system consisting of a two dimensional airfoil with a trailing edge flap. A mathematical model for the physical system considered here is formulated as a coupled system of ordinary differential and boundary integral equations. The coupling is described by the normal component of the airfoil velocity representing motions of the structure (which provide boundary conditions for the normal component of the flow velocity on the airfoil) and the resulting aerodynamic loads (forcing functions for the ordinary differential equations).

We note that mathematical models for the aeroelastic system have been studied quite extensively under the more restrictive “thin airfoil” assumption ([2], Section 5-4), to investigate active control strategies for flutter suppression in airfoils (see e.g. [1], [5], [6] and the references therein). In particular, the “thin airfoil” assumption, via an application of Söhngen’s inversion formula for finite Hilbert transforms ([7], [9]), leads to reformulations of the modeling equations in terms of a set of integro-differential equations of neutral- ([5]) or Volterra- ([1]) type which are used in the subsequent analysis and approximations in all the above mentioned references. It is not clear that the “inversion formula” based technique can be generalized for “non - thin” airfoils and therefore in this paper the equations governing the flow are solved directly in the exterior domain surrounding the airfoil using the boundary integral equation (BIE) method.

This work was supported in part by the Air Force Office of Scientific Research under grants F49620-92-J-0078 and F49620-93-1-0280

The BIE method is a “natural” candidate for this computational study, since it requires discretization of only the boundary (airfoil surface) to obtain approximations of the flow on the boundary. The pressure on the airfoil surface is the only flow information needed to compute approximations of the aerodynamic loads. Other approximation methods (e.g., the finite element method) would require repeated discretization of the flow domain, since the airfoil is in motion, and consequently the shape of the surrounding domain changes.

## 2. Model Description

A model for the aeroelastic system is described below. The model is formulated as a coupled system of ordinary differential equations, which describe the rigid body dynamics of the structure, and boundary integral equations, which describe the aerodynamics. The coupling occurs with the airfoil motion providing boundary conditions to the aerodynamics and the resulting aerodynamic loads providing forcing functions to the rigid body dynamics.

The rigid body dynamics are described by the quantities  $h$ ,  $\alpha$  and  $\beta$ , representing the plunge, pitch angle and flap angle, respectively (see Figure 1). Assuming small changes in these quantities, the dynamics of the system are given by the first order system

$$\dot{\mathbf{x}} = \mathbf{A}\mathbf{x} + \mathbf{F}(\phi(\mathbf{x}), \mathbf{x}), \quad (1)$$

where  $\mathbf{x} = [h, \alpha, \beta, \dot{h}, \dot{\alpha}, \dot{\beta}]^T$ ,  $\phi$  denotes the velocity potential for the flow,

$$\mathbf{A} = \begin{bmatrix} \mathbf{0} & \mathbf{I} \\ -\mathbf{M}^{-1}\mathbf{K} & \mathbf{0} \end{bmatrix} \quad (2)$$

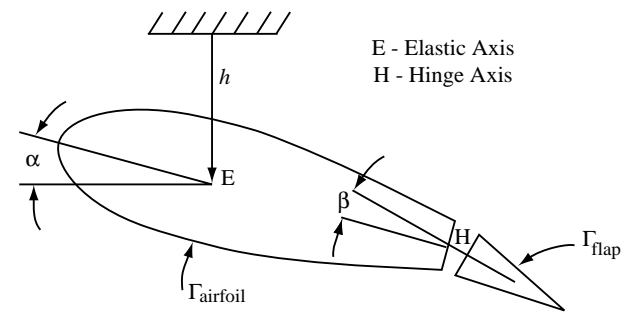


Figure 1. Airfoil Section Model

$$\mathbf{F}(\phi(\mathbf{x}), \mathbf{x}) = \begin{bmatrix} \mathbf{0} \\ \mathbf{M}^{-1} \mathbf{Q}(\phi(\mathbf{x}), \mathbf{x}) \end{bmatrix}, \quad (3)$$

with  $\mathbf{Q}(\phi(\mathbf{x}), \mathbf{x}) = [-L, -M_\alpha, -M_\beta]^T$  representing the aerodynamic loads. Note that the matrices  $\mathbf{M}$  and  $\mathbf{K}$  contain section parameters and spring constants which are provided in the appendix. The aerodynamic forces, i.e., lift ( $L$ ), pitching moment ( $M_\alpha$ ), and hinge moment ( $M_\beta$ ), as shown in Figure 2, can be obtained from the aerodynamic pressure,  $P$ , using the following expressions:

$$L = \int_{\Gamma} -P n_y d\Gamma, \quad M_\alpha = \int_{\Gamma} \mathbf{r}_E \times (-P \hat{\mathbf{n}}) d\Gamma \quad (4)$$

and

$$M_\beta = \int_{\Gamma_{\text{flap}}} \mathbf{r}_H \times (-P \hat{\mathbf{n}}) d\Gamma_{\text{flap}}. \quad (5)$$

Here,  $\hat{\mathbf{n}} \equiv n_x \hat{\mathbf{i}} + n_y \hat{\mathbf{j}}$  is the outward normal of the section surface,  $\Gamma = \Gamma_{\text{airfoil}} \cup \Gamma_{\text{flap}}$ , and  $\mathbf{r}_E$  and  $\mathbf{r}_H$  are vectors from the elastic axis and the hinge axis, respectively.

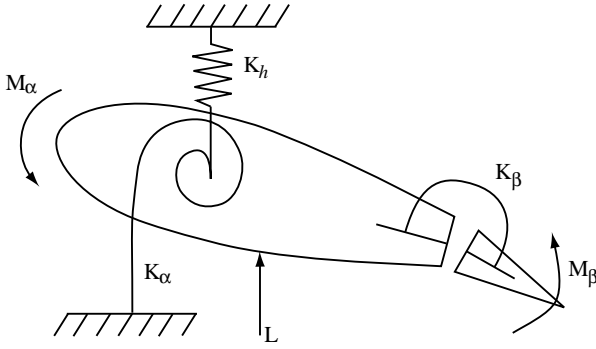


Figure 2. Aerodynamic Loads

For this model, we assume that the flow is unsteady, incompressible and irrotational. This last assumption allows us to introduce a scalar velocity potential function,  $\phi$ , from which the velocity is obtained using

$$\mathbf{V} \equiv u \hat{\mathbf{i}} + v \hat{\mathbf{j}} = \nabla \phi \equiv \frac{\partial \phi}{\partial x} \hat{\mathbf{i}} + \frac{\partial \phi}{\partial y} \hat{\mathbf{j}}. \quad (6)$$

The incompressible continuity equation leads to the fact that  $\phi$  satisfies the Laplace equation,

$$\nabla^2 \phi = 0, \quad (7)$$

in the exterior region surrounding the airfoil. In the far field, the flow is assumed to be uniform and to vary with time only, i.e.

$$\mathbf{V}_\infty = (u'_\infty(t) + U) \hat{\mathbf{i}} + v'_\infty(t) \hat{\mathbf{j}}. \quad (8)$$

where the subscript  $\infty$  refers to a value in the far field and the prime refers to a disturbance from the mean flow,  $\mathbf{V}_{\text{mean}} = U \hat{\mathbf{i}}$ . Therefore, the boundary conditions on the exterior boundary are

$$\frac{\partial \phi}{\partial x} = u'_\infty(t) + U \quad \text{and} \quad \frac{\partial \phi}{\partial y} = v'_\infty(t). \quad (9)$$

On the airfoil boundary, no flow penetrates the surface. Therefore the normal component of the flow velocity must match that of the airfoil. Thus, the structural motions are coupled to the aerodynamic behavior of the flow. This is expressed by,

$$\frac{\partial \phi}{\partial n} = \mathbf{V}_{\text{airfoil}} \cdot \hat{\mathbf{n}}. \quad (10)$$

For solving the exterior problem, with the far field boundary at infinity, we take advantage of the linearity of the Laplacian operator and use superposition. In doing so, we assume that  $\phi = \phi_1 + \phi_2$  and define

$$\phi_1 \equiv (U + u'_\infty(t))x + v'_\infty(t)y. \quad (11)$$

We see that  $\phi_1$  satisfies Laplace's equation and the desired boundary conditions on the exterior boundary. We now seek a solution to the Laplace equation,  $\phi_2$ , such that when the boundary conditions are added to those for  $\phi_1$ , we achieve the required conditions for  $\phi$ , given in equations (9) and (10). The boundary conditions for  $\phi_2$  are then given by

$$\phi_2 = 0 \quad (12)$$

at infinity, and

$$\frac{\partial \phi_2}{\partial n} = \mathbf{V}_{\text{airfoil}} \cdot \hat{\mathbf{n}} - (U + u'_\infty(t)) \frac{\partial x}{\partial n} - v'_\infty(t) \frac{\partial y}{\partial n} \quad (13)$$

on the airfoil surface. Laplace's equation for  $\phi_2$  with boundary conditions (12) and (13) can be reformulated (see [4], pages 85–89 or [8], pages 223–230 for details) as the boundary integral equation

$$c \phi'_2 + \int_{\Gamma} \phi'_2 \frac{\partial \phi^*}{\partial n} d\Gamma = \int_{\Gamma} \phi^* \frac{\partial \phi'_2}{\partial n} d\Gamma, \quad (14)$$

where  $\phi^*$  denotes the translation invariant fundamental solution for the Laplacian in two dimensions and is given by,

$$\phi^* = -\frac{1}{2\pi} \ln(\mathbf{r}),$$

where  $\mathbf{r}$  is the distance between the source and sample points, and  $c$  is the internal angle of the boundary at the source point (e.g.,  $c = \pi$  for a smooth boundary). Equation (14) can then be approximated using boundary elements as detailed in e.g. [4].

Once the (disturbance) velocity is determined (from some initial state with given far field flow disturbances), the surface pressure can be determined from the unsteady Bernoulli equation

$$\frac{\partial \phi}{\partial t} + \frac{P}{\rho} + \frac{1}{2} |\mathbf{V}|^2 = \frac{\partial \phi_\infty}{\partial t} + \frac{P_\infty}{\rho} + \frac{1}{2} |\mathbf{V}_\infty|^2,$$

and can be used to compute the aerodynamic loads in (4) and (5).

In this section, we consider control design for the aeroelastic model above by applying a torque at the flap-hinge. The dynamic equations for the controlled system are

$$\dot{\mathbf{x}} = \mathbf{A}\mathbf{x} + \mathbf{F}(\phi(\mathbf{x}), \mathbf{x}) + \mathbf{B}u \quad (15)$$

where

$$\mathbf{B} = \begin{bmatrix} \mathbf{0} \\ \mathbf{M}^{-1} \begin{bmatrix} 0 \\ 0 \\ 1 \end{bmatrix} \end{bmatrix} \quad (16)$$

and the control input,  $u$ , is determined using one of the following strategies.

For the first strategy, we experimented with the feedback control obtained by minimizing the cost functional

$$\mathcal{J}(u) = \int_0^\infty \{ \mathbf{x}^T \mathbf{Q} \mathbf{x} + u R u \} dt \quad (17)$$

subject to

$$\dot{\mathbf{x}} = \mathbf{A}\mathbf{x} + \mathbf{B}u. \quad (18)$$

In other words, we ignore the coupling term  $\mathbf{F}(\phi(\mathbf{x}))$ . This strategy seems to work well for this model since the coupling term is small in comparison to  $\mathbf{A}$ . This is true for slow mean flows, however may not work so well when the coupling is stronger.

The second strategy we explore is to include a first order approximation to  $\mathbf{F}(\phi(\mathbf{x}), \mathbf{x})$  in the control design, i.e. to minimize  $\mathcal{J}(u)$  subject to

$$\dot{\mathbf{x}} = (\mathbf{A} + \nabla \mathbf{F}(\phi(\mathbf{0}), \mathbf{0})) \mathbf{x} + \mathbf{B}u. \quad (19)$$

Hence some of the coupling is included. As a matter of fact,  $\mathbf{F}(\phi(\mathbf{x}), \mathbf{x}) \approx \nabla \mathbf{F}(\phi(\mathbf{0}), \mathbf{0})\mathbf{x}$  when there is no external flow disturbance. This is due to the fact that our simplified model of the aerodynamics predicts nearly linear aerodynamic loads for the small values of  $\mathbf{x}$  we consider.

Evaluation of the  $\nabla \mathbf{F}$  term was carried out using finite differences for this simplified flow model. However, for more complex flow models, where an evaluation of  $\mathbf{F}$  could be expensive, design sensitivities could be used. For example, an efficient approach to computing design sensitivities for the Euler equations was presented in [3].

#### 4. Numerical Results

In this section, we present some numerical results to test our control strategies. The system we consider consists of an NACA0009 airfoil section at a  $6^\circ$  angle of attack, where  $\alpha$  measures the deviation from this angle. The section parameters and spring constants for this example are given in the appendix.

Two flow cases are considered. In the first case, the mean flow is 440ft/s. The strength of the mean flow affects the magnitude of the coupling term as shown in the computations below. The flow disturbance is given as a

10ft/s increase in the mean flow for 0.1 seconds, in order to simulate a gust, i.e.

$$u'_\infty(t) = \begin{cases} 10\text{ft/s} & 0 \leq t \leq 0.1 \\ 0\text{ft/s} & 0.1 < t \end{cases} \quad (20)$$

and  $v'_\infty(t) = 0$ .

The feedback control,  $u = \mathbf{k}^T \mathbf{x}$ , is constructed by choosing  $\mathbf{Q} = \text{diag}(10^4, 10^4, 1, 1, 1, 1)$  and  $R = 0.0001$ . MATLAB was used to construct the gain matrix for the first control strategy (where the coupling term is neglected). The evolution of the controlled system (dashed line) and the uncontrolled system (solid line) are presented in Figures 3-5 for case 1. We observe that this control has a significant effect on controlling the pitch angle ( $\alpha$ ) and has a stabilizing effect on the plunge ( $h$ ), due to our choice of  $\mathbf{Q}$ . The larger values of  $\beta$  correspond to the application of the control.

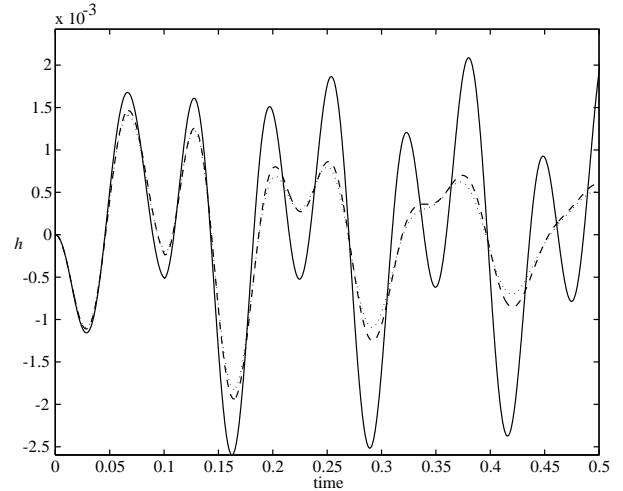


Figure 3. Case 1 - Plunge History

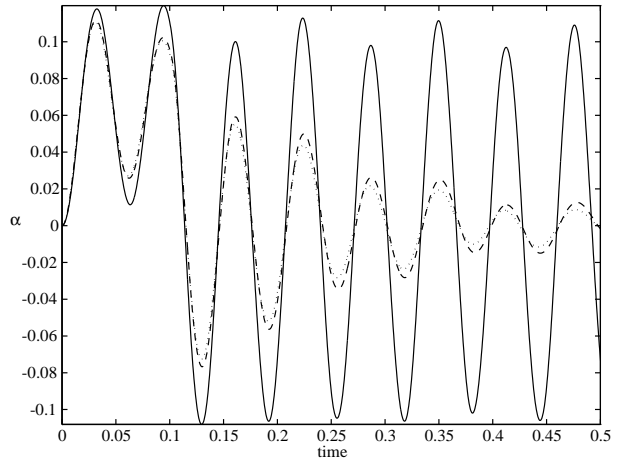


Figure 4. Case 1 - Pitch Angle History

For the second control strategy, the coupling term  $\mathbf{F}$  is linearized about the steady state:  $\mathbf{x} = \mathbf{0}$ ,  $U = 440\text{ft/s}$ ,  $u'_\infty = v'_\infty = 0$ . Using finite differences, we compute the gradient as

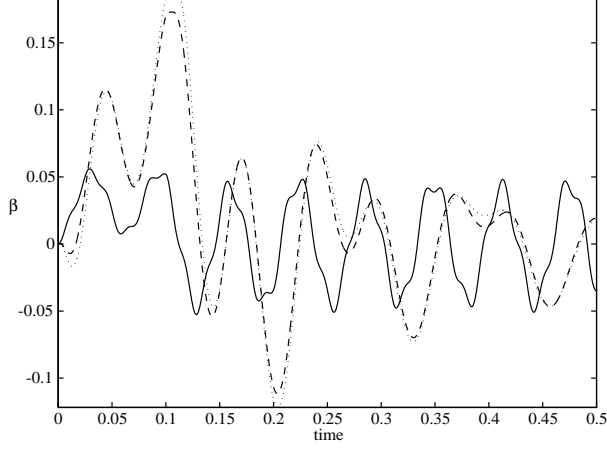


Figure 5. Case 1 - Flap Angle History

$\nabla\mathbf{F}(\phi(\mathbf{0}), \mathbf{0}) =$

$$\begin{bmatrix} 0.0 & 0.0 & 0.0 & 0.0 & 0.0 & 0.0 \\ 0.0 & 0.0 & 0.0 & 0.0 & 0.0 & 0.0 \\ 0.0 & 0.0 & 0.0 & 0.0 & 0.0 & 0.0 \\ 0.0 & -1249.1 & -98.1 & -2.6 & -3.1 & -0.1 \\ 0.0 & 1938.7 & -77.1 & 4.0 & 2.1 & -0.2 \\ 0.0 & 2356.7 & 4070.7 & 5.7 & 31.7 & 5.0 \end{bmatrix}$$

The gradient computation was very insensitive to the selection of the step size. These values are relatively small in magnitude, compared to the system matrix,  $\mathbf{A} =$

$$\begin{bmatrix} 0.0 & 0.0 & 0.0 & 1.0 & 0.0 & 0.0 \\ 0.0 & 0.0 & 0.0 & 0.0 & 1.0 & 0.0 \\ 0.0 & 0.0 & 0.0 & 0.0 & 0.0 & 1.0 \\ -2971.6 & 7501.6 & -1037.7 & 0.0 & 0.0 & 0.0 \\ 830.8 & -15003.2 & 8993.6 & 0.0 & 0.0 & 0.0 \\ -511.2 & 40008.2 & -116225.6 & 0.0 & 0.0 & 0.0 \end{bmatrix}$$

The gain matrix, computed using  $(\mathbf{A} + \nabla\mathbf{F}(\phi(\mathbf{0}), \mathbf{0}))$  was used for case 1, and the simulation is also plotted (dotted line) in Figures 3-5. There is only a small improvement in the performance due to the weak coupling between the flow and the structure.

In the second case, the mean flow is increased ( $U = 600\text{ft/s}$ ) to generate more coupling between the systems. The evolution of the states are presented in Figures 6-8 for the uncontrolled system (solid line) and the controlled system, using the first control strategy which ignores the coupling term (dashed line). This control strategy still provides good behavior, however, now there is more improvement when the linearized coupling term,  $\nabla\mathbf{F}(\phi(\mathbf{0}), \mathbf{0}) =$

$$\begin{bmatrix} 0.0 & 0.0 & 0.0 & 0.0 & 0.0 & 0.0 \\ 0.0 & 0.0 & 0.0 & 0.0 & 0.0 & 0.0 \\ 0.0 & 0.0 & 0.0 & 0.0 & 0.0 & 0.0 \\ 0.0 & -2322.7 & -182.5 & -3.6 & -4.2 & -0.2 \\ 0.0 & 3605.0 & -143.3 & 5.5 & 2.9 & -0.2 \\ 0.0 & 4382.4 & 7569.5 & 7.7 & 43.2 & 6.8 \end{bmatrix}$$

is used in the control design. The effect of this control is plotted in Figures 6-8 (as the dotted line) and we see that it

has much more impact on the plunge and pitch angle than it did in the first case.

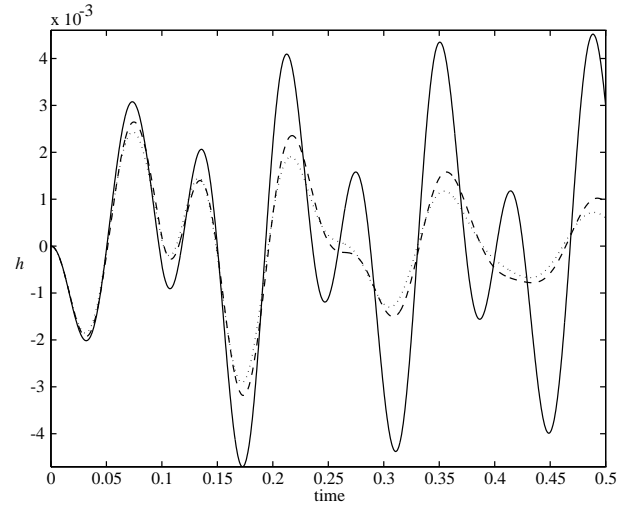


Figure 6. Case 2 - Plunge History

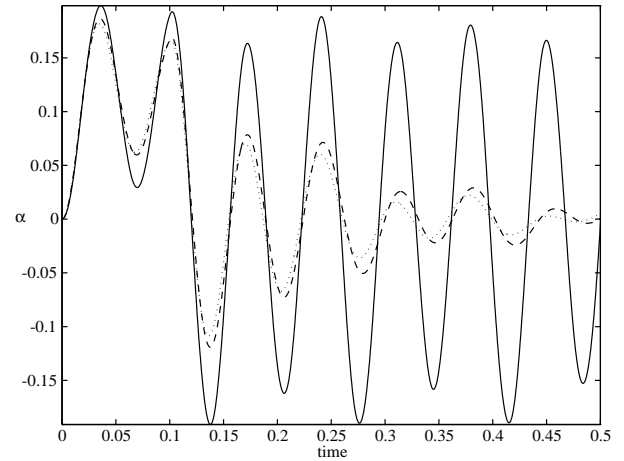


Figure 7. Case 2 - Pitch Angle History

## 5. Conclusions

In this paper, we presented a model of an aeroelastic system which is an effective tool in studying flow induced vibrations. Disturbance attenuation by the application of a hinge line torque is studied using two control strategies. The control strategy which included a linearization of the coupling term showed some improvement over the strategy where the coupling was ignored. It should also be noted that more elaborate control strategies would not generate significant improvement due to the fact that the coupling term is essentially linear near the zero state and the coupling term is weak at the flow speeds tested.

A natural extension of this work would be to use a more complex flow model (e.g. the Euler equations). The effectiveness of the control strategies presented here could be studied for this new model and could suggest whether more complex strategies are needed. Such an extension

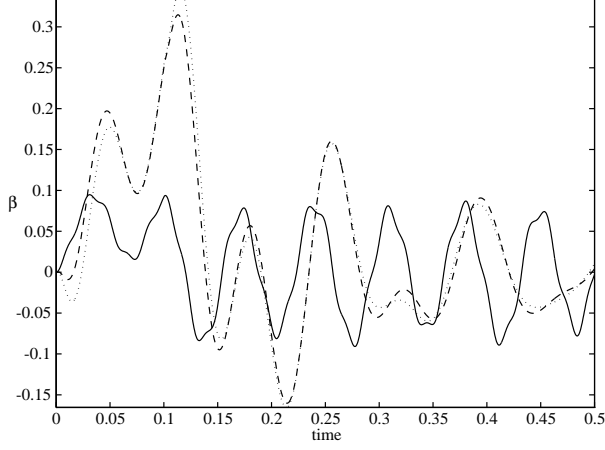


Figure 8. Case 2 - Flap Angle History

represents a significant departure from this work, which takes advantage of the boundary integral equation method to efficiently solve the flow equations.

### References

- [1] A. V. Balakrishnan. Active control of airfoils in unsteady aerodynamics. *Applied Mathematics and Optimization*, 4(2):171–195, 1978.
- [2] R. L. Bisplinghoff, H. Ashley, and R. L. Halfman. *Aeroelasticity*. Addison-Wesley, Cambridge, MA, 1955.
- [3] J. Borggaard, J. Burns, E. Cliff, and M. Gunzburger. Sensitivity calculations for a 2d, inviscid, supersonic forebody problem. In H. T. Banks, R. Fabiano, and K. Ito, editors, *Identification and Control of Systems Governed by Partial Differential Equations*. SIAM Publications, 1993.
- [4] C. A. Brebbia, J. C. F. Telles, and L. C. Wrobel. *Boundary Element Techniques*. Springer-Verlag, Berlin, 1984.
- [5] J. A. Burns, E. M. Cliff, and T. L. Herdman. A state-space model for an aeroelastic system. In *Proceedings of the 22nd IEEE Conference on Decision and Control*, volume 3, pages 1074–1077, San Antonio, TX, 1983.
- [6] J. W. Edwards. *Unsteady Aerodynamic Modeling and Active Aeroelastic Control*. PhD thesis, Stanford University, 1977.
- [7] T. L. Herdman and J. Turi. An application of finite hilbert transforms in the derivation of a state space model for an aeroelastic system. *Journal of Integral Equations and Applications*, 3(2):271–287, 1991.
- [8] A. H. Schatz, V. Thomee, and W. L. Wendland. *Mathematical Theory of Finite and Boundary Element Methods*. Birkhauser Verlag, Basel, 1990.
- [9] F. G. Tricomi. *Integral Equations*. Interscience, New York, 1957.
- [10] D. L. York. Analysis of flutter and flutter suppression via an energy method. Master's thesis, Virginia Polytechnic Institute and State University, May 1980.

### Appendix

Following the notation in [6], for sufficiently small  $\alpha$ , the matrices  $\mathbf{M}$  and  $\mathbf{K}$  are composed of airfoil section parameters as follows:

$$\mathbf{M} = \begin{bmatrix} m & S_\alpha & S_\beta \\ S_\alpha & I_\alpha & I_\beta + cS_\beta \\ S_\beta & I_\beta + cS_\beta & I_\beta \end{bmatrix}$$

$$\mathbf{K} = \begin{bmatrix} K_h & 0 & 0 \\ 0 & K_\alpha & 0 \\ 0 & 0 & K_\beta \end{bmatrix}.$$

The numerical values for these section parameters were taken from [10] and are tabulated below,

$$\begin{aligned} m &= 2.6883 \frac{\text{slugs}}{\text{ft}} & S_\alpha &= 1.61298 \text{ slugs} \\ K_h &= 6,700 \frac{\text{slugs}}{\text{ft-s}^2} & S_\beta &= 0.10081 \text{ slugs} \\ K_\alpha &= 60,500 \frac{\text{slugs}}{\text{ft-s}^2} & I_\alpha &= 6.04868 \frac{\text{slugs-ft}^2}{\text{ft}} \\ K_\beta &= 13,600 \frac{\text{slugs}}{\text{ft-s}^2} & I_\beta &= 0.151217 \frac{\text{slugs-ft}^2}{\text{ft}} \end{aligned}$$

where  $c = 3$  ft is the distance from the elastic axis to the hinge axis.

Using these values in the expressions for  $\mathbf{M}$  and  $\mathbf{K}$ , we compute the system matrix  $\mathbf{A}$ . The eigenvalues for this matrix are:  $\pm 48.6965 i$ ,  $\pm 110.2448 i$  and  $\pm 345.9415 i$ .